Turkish Journal of Electrical Engineering & Computer Sciences

http://journals.tubitak.gov.tr/elektrik/

Research Article

Turk J Elec Eng & Comp Sci
(2017) 25: 2261 – 2277

doi:10.3906/elk-1604-102

Novel control strategy for hybrid renewable energy-based standalone system

Rahul SHARMA*, Sathans SUHAG
Department of Electrical Engineering, National Institute of Technology, Kurukshetra, India

Received: 09.04.2016 • **Accepted/Published Online:** 29.08.2016 • **Final Version:** 29.05.2017

Abstract: In this paper, novel control strategies are proposed for a hybrid renewable energy system under a standalone environment. The wind unit, solar unit, supercapacitor (SC), and battery are connected to a DC link through power converters. Control methods are proposed to mitigate the limitations of the standalone system. The control method is proposed to maintain constant DC link voltage under different conditions without using a dummy load (i.e. an electrolyzer). The SC and battery are used as storage devices. A novel control scheme is proposed to control storage devices where the SC is used to improve the slow response of the system under battery storage. A novel optimal power point tracking control algorithm is proposed in place of maximum power point tracking to provide the demanded power without using extra components and control. Simulation results under different environmental and operating conditions are presented.

Key words: Renewable energy, storage devices, standalone system, maximum power point tracking, optimal power point tracking

1. Introduction

In today's world, efficient use of renewable energy sources is becoming increasingly important due to increase in demand of energy consumption and limited sources of fossil fuel. In remote areas, renewable energy sources are the most promising option where connection to a utility grid is not feasible. In such areas, renewable energy systems offer the best solutions for power generation [1,2]. Standalone renewable energy systems based on one source also have limitations. To ensure a continuous power supply, a more reliable solution employs a hybrid renewable energy system (HRES)-based microgrid. However, there are many control challenges that need to be addressed in order to make a standalone HRES more reliable and cost-effective with improved power quality [3]. To improve power quality much attention is needed to mitigate the problem of voltage variation that occurs due to change in loads and flickers introduced due to unpredictable changes in source input like variations in wind speed and solar irradiance [4,5]. The aforesaid power quality issues must be addressed to provide better quality power. Therefore, this paper proposes novel control strategies to address the power quality problems mentioned above.

Based on a similar HRES, papers have recently been presented by a few authors. In [6], battery storage system-based control was proposed for smoothing the DC link voltage but an inverter is also used in the same control, which increases the extra components in the system and hence increases the cost and complexity as well. A renewable energy-based DC microgrid system was presented in [7], wherein a control method for different conditions is proposed, but it does not mention the control for DC link voltage regulation in a situation where

*Correspondence: rahulsharma.knit2006@gmail.com

storage devices are fully charged and the power generated by the source is more than the demanded power. In [8], a hybrid standalone system was proposed to regulate DC link voltage, but the authors compromised the quality of power by considering 40–50 V variation in DC link voltage as acceptable besides using power converter-based dump load, which is also an extra component required. In [9], the authors reviewed the control of a hybrid microgrid under islanded conditions but did not cover the control technique to regulate DC link voltage when surplus power is available in islanded conditions. In [10], control was developed to consider linear DC loads only and the authors did not consider voltage instability problems when violations of the limits of the state of charge in the storage system occur. In [11], the authors proposed a battery charge/discharge controller to maintain DC link voltage but did not consider AC loads, nonlinear loads, or a control mechanism in the event of surplus power if the battery is fully charged. In [12], the authors presented an investigation to control transient power under an islanded microgrid but only used a battery bank as a storage device, which has slow charging/discharging. Hence, the response of the system is slow under transient conditions, the remedy of which is not discussed in the paper. In [13], the authors addressed most of the problems except that the control is not able to regulate DC link voltage under non-MPPT mode and the voltage varies from 70 to 80 V, which is not acceptable as per power quality standards.

This work proposes control strategies to address the aforesaid power quality problems of a standalone system under different conditions. No similar work has been reported in the literature to date. The HRES consists of a permanent magnet synchronous generator (PMSG)-based wind system, a photovoltaic (PV) panel, a SC, and a battery storage system, as shown in Figure 1.

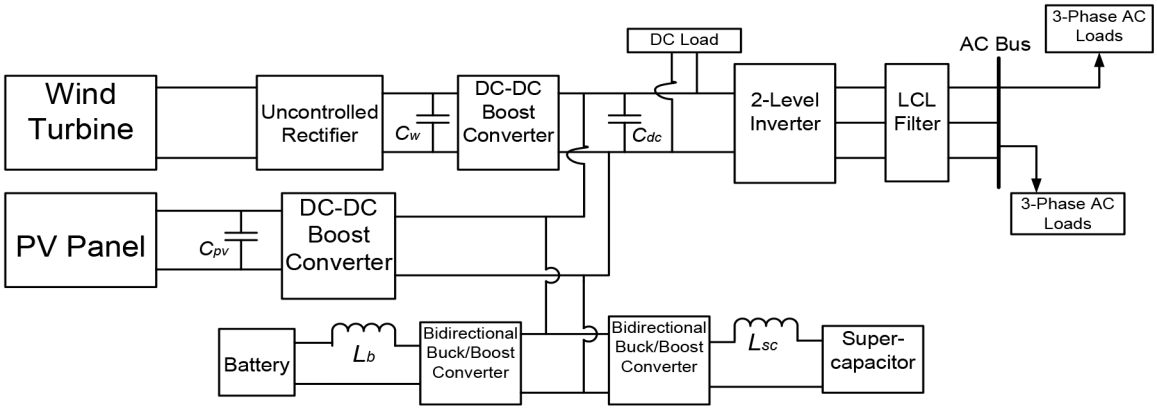

Figure 1. Standalone hybrid energy system.

Solar and wind sources are connected to respective boost converters to achieve OPPT in place of MPPT. The battery and SC are used as storage devices and connected to a DC link through DC-DC bidirectional converters. DC loads are directly connected to the DC link bus and AC loads are connected to the DC link through an inverter.

The SC is used to improve the slow response of the storage system as well as to improve the life span and reduce the size and stress of the battery due to slow charging/discharging rate, similarly to [14,15], but with a better proposed control strategy and thereby improved response. In this paper, control strategies are developed to:

1. Achieve OPPT control, which eliminates the use of power converter-based dummy load and hence reduces the cost of the system.

2. Maintain constant DC link voltage irrespective of changes in system conditions.

3. Control the battery and SC using DC-DC bidirectional converters for fast dynamic response as compared to conventional control.

4. Obtain a coordinated control algorithm between the wind unit, PV unit, battery, and SC for optimal power flow.

This paper is divided into five sections as follows: in Section 2, detailed modeling of the HRES under standalone condition is discussed. Section 3 covers the proposed control strategies for OPPT, the method for control of charging/discharging of storage devices, inverter control, and a coordinated control algorithm for DC voltage regulation. Section 4 presents the results obtained under different conditions and a discussion on the outcomes with proposed control strategies. Section 5 concludes the findings of this study on the HRES in a standalone environment with the proposed novel control strategies.

2. Modeling of the hybrid renewable energy system

The HRES is modeled to design the controllers. PV and wind turbine modeling was already reported in various studies [16,17]. Only the modeling of storage devices with a buck/boost converter and inverter with inductance-capacitance-inductance (LCL) filter is discussed in this paper.

2.1. Modeling of battery and SC with bidirectional buck/boost converter

Figure 2 shows the scheme of the battery and SC connected to the bidirectional buck/boost converter as an energy storage system.

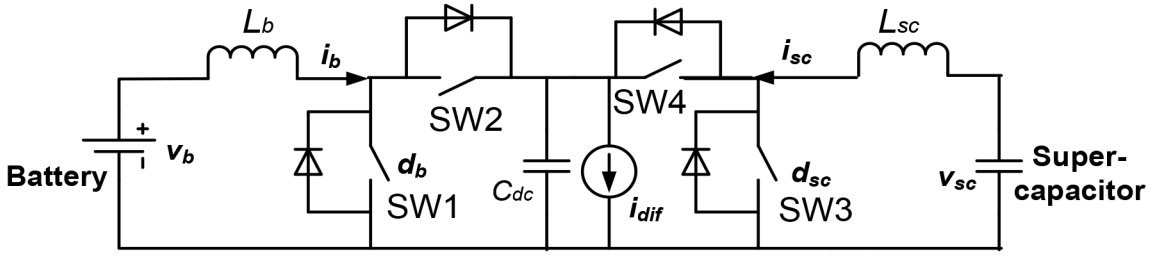

Figure 2. Basic circuit model of energy storage system.

In this system, neglecting the switching losses and using the volt-second principle, the time average model of the energy storage system can be obtained as follows:

$$L_b \frac{di_b}{dt} = v_b - (1 - d_b)v_{dc}, \tag{1}$$

$$L_{sc} \frac{di_{sc}}{dt} = v_{sc} - (1 - d_{sc})v_{dc}, \tag{2}$$

where L_b, L_{sc} are filter inductances, v_b, v_{sc} are voltages, and d_b, d_{sc} are duty cycles of the battery and SC, respectively. v_{dc} is the DC link voltage of the capacitor.

Based on the instantaneous power, the balance condition between the source and load through the DC link can be expressed by the following differential equation as:

$$v_{dc}C_{dc}\frac{dv_{dc}}{dt} = p_{source} - p_{load} \tag{3}$$

where C_{dc} is the capacitance of the DC link, p_{source} is the input power to the DC link by all sources, and p_{load} is the output power of the DC link consumed by DC and AC loads.

$$i_{dif} = \frac{p_{pv} + p_w - p_{load}}{v_{dc}} \tag{4}$$

Furthermore,

$$p_{pv} + p_w + p_b + p_{sc} = p_{source}, \tag{5}$$

where p_{pv}, p_w, p_b, p_{sc} are the output powers of the PV panel, wind turbine, battery, and SC, respectively.

2.2. Modeling of three-phase inverter with LCL filter

A three-phase inverter with LCL filter is modeled in Figure 3, where the injected current into the AC bus is i_2, while v_{dc} is the DC link voltage across the capacitance C_{dc} and C_f is the filter capacitance. The LCL filter design is implemented as per [18] to interface the inverter to the AC bus.

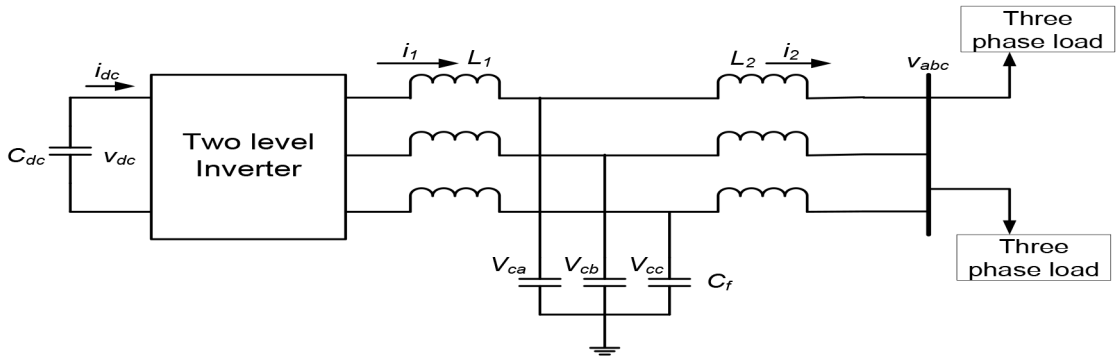

Figure 3. Three-phase inverter with LCL filter.

In the steady state, the controlled three-phase AC bus current is i_{2abc} and voltage is v_{abc}. After transformation, with the help of the LCL filter, the system differential equations in the synchronous reference $(d-q)$ frame are as follows:

$$L_1\frac{di_{1d}}{dt} = L_1\omega i_{1q} + v_{id} - v_{cd}, \tag{6}$$

$$L_1\frac{di_{1q}}{dt} = -L_1\omega i_{1d} + v_{iq} - v_{cq}, \tag{7}$$

$$C_f\frac{dv_{cd}}{dt} = -C_f\omega v_{cq} + i_{1d} - i_{2d}, \tag{8}$$

$$C_f\frac{dV_{cq}}{dt} = C_f\omega V_{cd} + I_{1q} - I_{2q}, \tag{9}$$

$$L_2 \frac{di_{2q}}{dt} = L_2 \omega i_{2d} + v_{cq}, \tag{10}$$

and the system input variables are expressed as $u = \begin{bmatrix} u_d & u_q \end{bmatrix}$, where

$$\begin{aligned} v_{id} &= \sqrt{3/8} v_{dc} u_d \\ v_{iq} &= \sqrt{3/8} v_{dc} u_q \end{aligned} . \tag{11}$$

In the next section, using the above equations, the proposed control scheme will be discussed.

3. Control design of hybrid energy system

3.1. Optimal power point tracking control of PV system

The OPPT control algorithm is proposed to extract optimum PV power using a DC-DC boost converter in place of MPPT control, as in Figure 4.

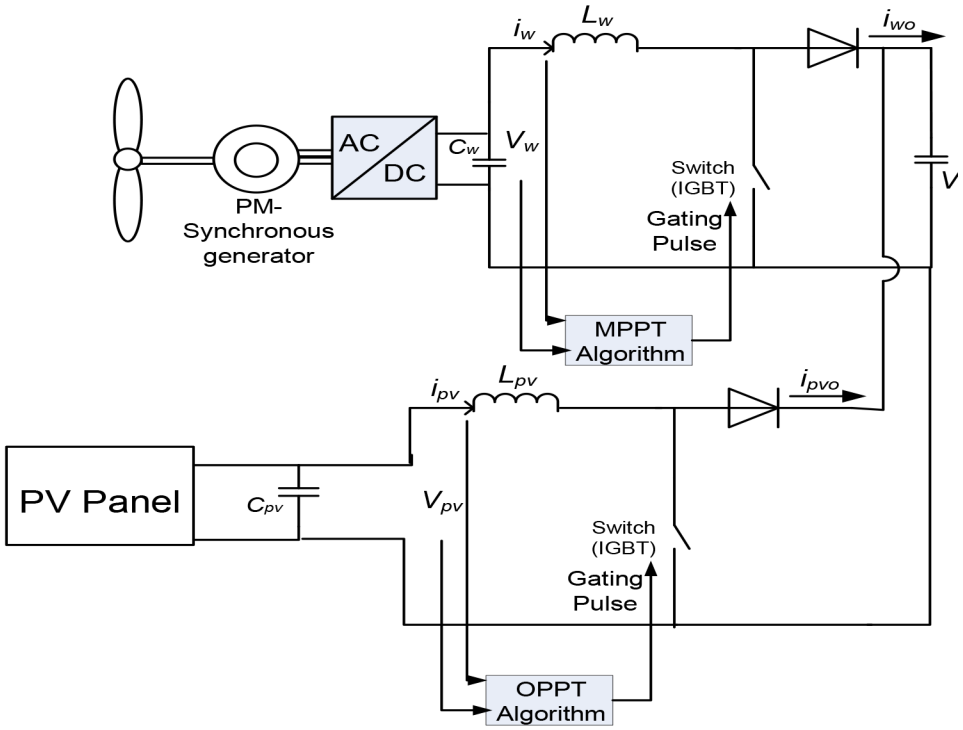

Figure 4. Circuit for control of wind and PV system.

To maintain constant DC link voltage at the reference value, power must be balanced across the DC link as follows:

$$p_{pv} + p_w = p_{load} \pm (p_b + p_{sc}),$$

where $-(p_b + p_{sc})$ under charging if $p_{pv} + p_w > p_{load}$ and $+(p_b + p_{sc})$ under discharging condition if $p_{pv} + p_w < p_{load}$ to balance power across the DC link.

Now, under charging conditions, if the storage devices are fully charged then they will be disconnected; therefore, $-(p_b + p_{sc}) = 0$ and unbalanced power across the DC link can be written as $p_{pv} + p_w > p_{load}$. Under this condition, the DC link voltage is not able to be maintained as constant. To avoid a power unbalancing situation, a conventional approach is used for controlled dummy load to dump the extra generated power Δp, where $\Delta p = (p_{pv} + p_w) - p_{load}$. The dummy load can balance the power but has adverse effects that introduce switching loss and ripples in the DC link voltage as well as being an extra component, which increases the cost of the system.

In this paper, an OPPT control algorithm is proposed to solve the aforementioned problem. MPPT control extracts maximum power irrespective of power requirements, which requires the controlled dummy load to balance the power, whereas OPPT control extracts the required power by changing the operating point for the PV characteristics. OPPT control can change the generated power to maintain a balance across the DC link, which helps to maintain the DC link voltage constant without any dummy load requirement. It reduces generated power by Δp with the help of PV characteristics as shown in Figure 5 to balance the power across the DC link.

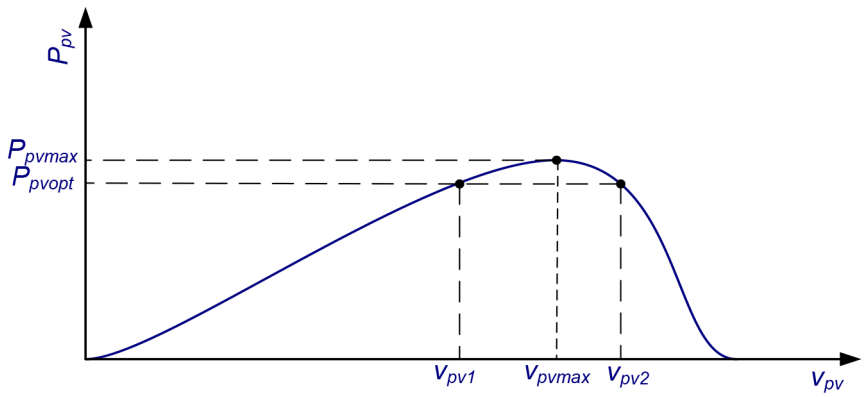

Figure 5. Characteristics of PV system.

OPPT extracts maximum power when storage devices are not fully charged, but when an overcharging condition occurs, OPPT extracts optimum power to balance the power across the DC link based on the load requirement instead of maximum power and hence maintains the DC link voltage constant at the reference point.

To reduce extra power ($\Delta p = p_{pvmax} - p_{pvopt}$), OPPT shifts the operating point from maximum power point p_{pvmax} to optimum point p_{pvopt} when the generated power is more than the required power and the state of charge (SOC) is above 0.9. To reduce the generated power, OPPT shifts the operating point towards the left by increasing the duty cycle of the boost converter in steps according to the OPPT algorithm as explained in the flowchart in Figure 6. In this control, only voltage and current measurement is needed to control OPPT, just like MPPT. The difference in the OPPT algorithm is that it can shift the operating point from the maximum value of power to an optimum value, while in MPPT, the operating point is always at the maximum value of power. OPPT control also operates at maximum power if storage devices are not fully charged, just like MPPT, but when storage devices are fully charged (disconnected), OPPT shifts the operating point to balance power across the DC link while MPPT always operates at the maximum point, which unbalances the power across the DC link.

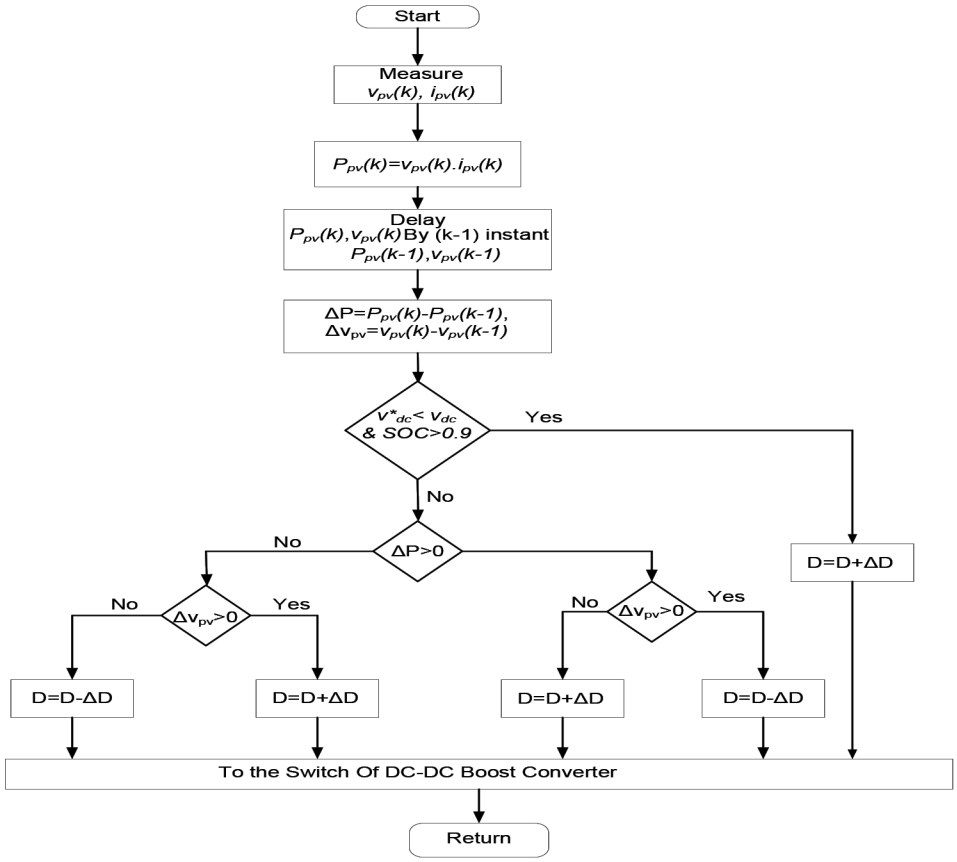

Figure 6. Control algorithm of OPPT control for PV system.

3.2. Control design of the battery and SC using bidirectional buck/boost converter

In control design for energy storage devices, charging/discharging is considered under the limits of the SOC. The basic concept of this control is that the battery supports slow transients and the SC supports fast transients. Therefore, the error between reference DC voltage and actual DC voltage acts as input to the proportional-integral (PI) controller whose output controls the total current that is to be supplied by the energy storage devices. The total current can be divided into two parts using a low-pass filter (LPF) to generate a dynamic component, which gives reference current to the SC control loop, and an average component that gives reference current to the battery control loop. This type of control strategy was reported in [19] but this control strategy does not consider the slow dynamics of the battery to compensate for the battery error current, which increases the time to settle down the DC-link voltage at the reference point. In the proposed control scheme, voltage and the current control loops are designed using feedback linearization theory to improve the dynamics of the control strategy. Detailed theory on feedback linearization can be found in [20]; it is applied to design the proposed control scheme to maintain the constant DC-link voltage.

By substituting Eqs. (4) and (5) in Eq. (3), we get:

$$v_{dc}C_{dc}\frac{dv_{dc}}{dt} = p_{sc} + p_b + i_{dif}v_{dc}. \tag{12}$$

When the feedback linearization technique is employed for Eq. (12), we get:

$$i_{dif} = \lambda^{-1}(x)\left[-\mu(x) + V\right], \tag{13}$$

where $\lambda^{-1}(x) = \frac{C_{dc}}{v_{dc}}$, $\mu(x) = \frac{p_b + p_{sc}}{C_{dc}}$ and $V = \frac{1}{2}(\dot{v}_{dc}^2)$.

Similarly, using Eqs. (1) and (2), we get:

$$\begin{bmatrix} \dot{i}_b \\ \dot{i}_{sc} \end{bmatrix} = \begin{bmatrix} \frac{v_b - v_{dc}}{L_b} \\ \frac{v_{sc} - v_{dc}}{L_{sc}} \end{bmatrix} + \begin{bmatrix} \frac{v_{dc}}{L_b} & 0 \\ 0 & \frac{v_{dc}}{L_{sc}} \end{bmatrix} \begin{bmatrix} d_b \\ d_{sc} \end{bmatrix}. \tag{14}$$

After applying the feedback linearization technique, we get:

$$\begin{bmatrix} d_b \\ d_{sc} \end{bmatrix} = \begin{bmatrix} \frac{L_b}{v_{dc}} & 0 \\ 0 & \frac{L_{sc}}{v_{dc}} \end{bmatrix} \left\{ - \begin{bmatrix} \frac{v_b - v_{dc}}{L_b} \\ \frac{v_{sc} - v_{dc}}{L_{sc}} \end{bmatrix} + \begin{bmatrix} V_1 \\ V_2 \end{bmatrix} \right\}, \tag{15}$$

where $\lambda^{-1}(x) = \begin{bmatrix} \frac{L_b}{v_{dc}} & 0 \\ 0 & \frac{L_{sc}}{v_{dc}} \end{bmatrix}$, $\mu(x) = \begin{bmatrix} \frac{v_b - v_{dc}}{L_b} \\ \frac{v_{sc} - v_{dc}}{L_{sc}} \end{bmatrix}$, and $\begin{bmatrix} V_1 \\ V_2 \end{bmatrix} = \begin{bmatrix} \dot{i}_b \\ \dot{i}_{sc} \end{bmatrix}$.

Linear control laws are designed using the PI controller for Eqs. (13) and (15).

In the proposed control scheme, i^*_{dif} is the total current required to be fed from the battery and SC, obtained from the voltage control loop using Eq. (12). The total required current is separated into a dynamic component and average component using the LPF. The average component is the reference current i^*_b of the battery and the dynamic component must be the reference current of the SC control loop. However, the battery has slow dynamics and therefore error in battery power can be compensated using the SC to improve the dynamics of the control scheme, which in turn changes the reference current i^*_{sc} of the SC control loop.

$$(i^*_b - i_b)v_b = p_{uncomp\_b}, \tag{16}$$

where p_{uncomp_b} is the power needed to be compensated using the battery control loop. To improve dynamics, however, it has to be compensated using the SC control loop. Hence, power compensated using the SC control loop is:

$$(i^*_b - i_b)v_b + (i^*_{dif} - i^*_b)v_{sc} = p_{comp\_sc}, \tag{17}$$

$$p_{comp\_sc} = i^*_{sc}v_{sc}, \tag{18}$$

and therefore

$$i^*_{sc} = (i^*_b - i_b)\frac{v_b}{v_{sc}} + (i^*_{dif} - i^*_b). \tag{19}$$

The reference current i^*_{sc} of the SC includes error of the battery to improve the dynamic response. With the help of Eqs. (13), (15), and (19), a control scheme is designed as in Figure 7.

This scheme provides robust and improved dynamic tracking with minimum steady-state error besides disturbance rejection as compared to the conventional one.

Now a coordinated control algorithm is presented as in Figure 8 to switch the control of storage devices from charging mode to discharging mode and floating (disconnected) mode (neither charging nor discharging)

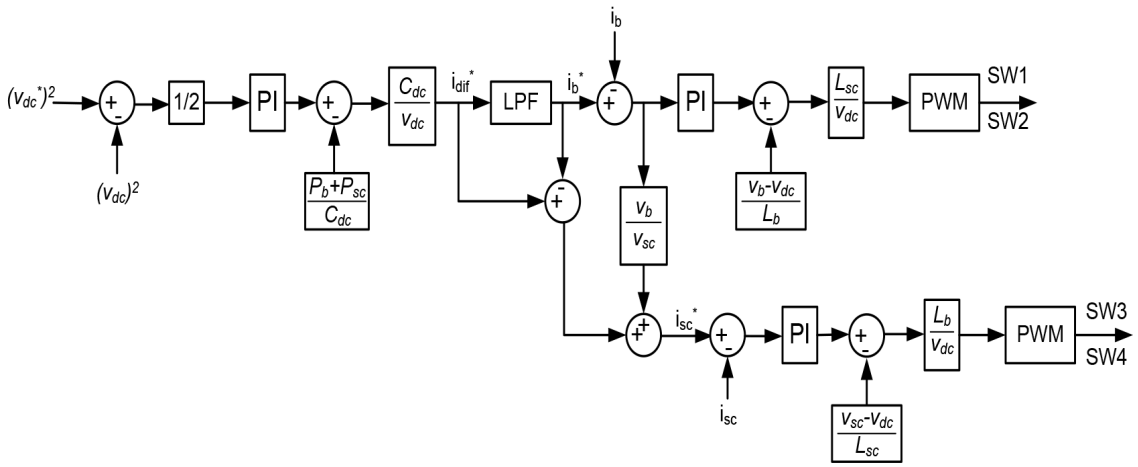

Figure 7. Proposed control scheme for energy storage devices.

in the case of overcharging. Switches SW1 and SW3 are controlled by pulse width modulation (PWM) in discharging mode of the battery and SC while SW2 and SW4 are controlled by PWM in charging mode and SW1 and SW2 are off when the battery is in floating mode while the SC remains connected under overcharging condition due to overcharging capacity but negligible charging current keeps flowing. The SC, under this situation, is not able to regulate the DC link voltage. The battery must not work above or below SOC limits; otherwise, the lifespan gets reduced, the stress gets increased, and the working performance of the battery is adversely affected. The proposed control algorithm, therefore, changes the mode of operation of storage devices under different conditions by taking the SOC within limits.

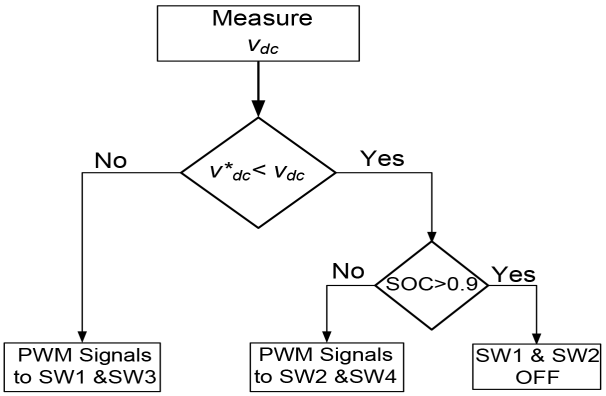

Figure 8. Coordinated control scheme algorithm.

3.3. Control design for three-phase inverter with LCL filter

The proposed control scheme is designed using Eqs. (6) to (11) by applying a feedback linearization technique to obtain constant AC voltage and improved power factor at the AC bus.

The first step is to design closed loop control using i_{1d} and i_{1q} as output and v_{id} and v_{iq} as input variables. Now the differential equations of Eqs. (6) and (7) can be written as:

$$\begin{bmatrix} \dot{i}_{1d} \\ \dot{i}_{1q} \end{bmatrix} = \begin{bmatrix} \omega i_{1q} - v_{cd}/L_1 \\ -\omega i_{1d} - v_{cq}/L_1 \end{bmatrix} + \begin{bmatrix} 1/L_1 & 0 \\ 0 & 1/L_1 \end{bmatrix} \begin{bmatrix} v_{id} \\ v_{iq} \end{bmatrix} and \begin{bmatrix} y_1 \\ y_2 \end{bmatrix} = \begin{bmatrix} i_{1d} \\ i_{1q} \end{bmatrix}. \tag{20}$$

Now, using feedback linearization, the above equations can be rewritten as:

$$\begin{aligned} \dot{y}_1 &= \omega i_{1q} - v_{cd}/L_1 + v_{id}/L_1 \\ \dot{y}_2 &= -\omega i_{1d} - v_{cq}/L_1 + v_{iq}/L_1 \end{aligned}, \tag{21}$$

$$\begin{bmatrix} v_{id} \\ v_{iq} \end{bmatrix} = \begin{bmatrix} L_1 & 0 \\ 0 & L_1 \end{bmatrix} \begin{bmatrix} -(\omega i_{1q} - v_{cd}/L_1) + V_1 \\ (\omega i_{1d} + v_{cq}/L_1) + V_2 \end{bmatrix}. \tag{22}$$

Eq. (21) can be written as Eq. (22), where V_1 and V_2 are the synthetic inputs.

Subsequently, in the next step, the feedback linearization technique is applied for closed loop control of v_{cd} and v_{cq} as output variables and i_{1d} and i_{1q} as input variables, which are assumed to be equal to the reference values (desired outputs).

The differential equations of Eqs. (8) and (9) can be expressed using feedback linearization; the closed loop control is written as:

$$\begin{bmatrix} i_{1d} \\ i_{1q} \end{bmatrix} = \begin{bmatrix} C_f & 0 \\ 0 & C_f \end{bmatrix} \begin{bmatrix} -(\omega v_{cq} - i_{2d}/C_f) + V_3 \\ (\omega v_{cd} + i_{2q}/C_f) + V_4 \end{bmatrix}. \tag{23}$$

Similarly, feedback linearization is applied in Eq. (10) to obtain the reference of v_{cq} and the desired output to control the reactive power. Active power is already controlled using energy storage devices. Therefore, the v_{cd} reference is calculated as per the required output AC bus voltage. Similarly, reference current $i*_{2q}$ and actual current i_{2q} are used to regulate reactive power control and obtain an improved power factor at the AC bus.

The equation can be written as

$$v_{cq} = L_2 \left\{ -\omega i_{2d} + V_5 \right\}. \tag{24}$$

Now, using Eqs. (22), (23), and (24), the control scheme is designed for the inverter.

Inverter switching is controlled by the control scheme based on the feedback linearization control technique as in Figure 9.

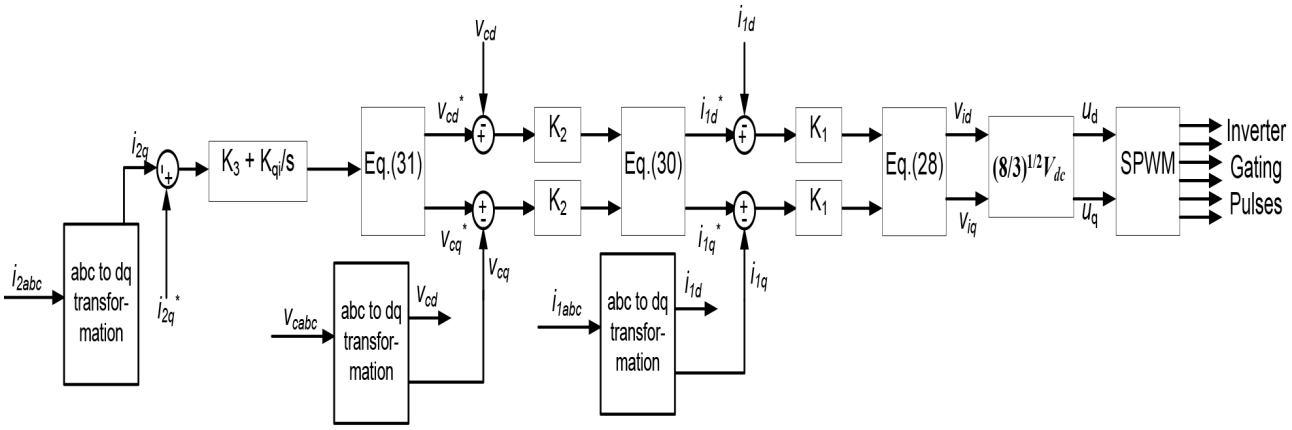

Figure 9. Control scheme of three-phase inverter.

To get the desired output in terms of AC bus voltage and power factor, inverter switches are controlled by controlling the outputs of the d- and q-axis, which are used as reference waves in sinusoidal PWM to generate gating signals for inverter switches.

4. Results and discussion

The proposed control strategies have been implemented in a 15-kW hybrid renewable energy system under standalone condition. To demonstrate the performance of the proposed control strategies, the system is simulated in MATLAB under different operating conditions. The system parameters are given in Tables 1 and 2.

Table 1. Storage devices parameters.

Battery	Lead acid - 12 V, 20 Ah, 20 no. connected in series
Supercapacitor	58 F, 16 V, 10 no. connected in series
L_b	6 mH
L_{sc}	5 mH
v_b	240 V
v_{sc}	160 V

Table 2. Nominal system parameters.

Wind system rating	10 kW
PV system rating	5 kW
AC bus voltage rating, v_p	170 V
C_{pv}	100 μF
C_w	150 μF
L_{pv}	5 mH
L_w	7 mH
C_{dc}	1000 μF
L_1	0.35 mH
L_2	0.1 mH
C_f	120 μF

Solar irradiance and wind speed changes are introduced to study the system performance under different environmental conditions and load change is introduced to assess the system performance under different operating conditions. Results are discussed under different system conditions in the time zone from 0 s to 6 s. Different system conditions are simulated using variable irradiance of the PV system as in Figure 10 and variable wind speed as in Figure 11.

The load variation pattern is as shown in Figure 12. It can be seen that the PV power and wind power are in accordance with the variations in the solar irradiance and wind speed, respectively. Figure 12 shows the variation of wind power, PV power, and load power from 0 s to 6 s. As can be seen, wind and PV combined total power is 7.9 kW, whereas load power is 9 kW from 0 s to 1 s. In this period, storage devices are in discharging mode to compensate for the imbalance between total power and the load demand.

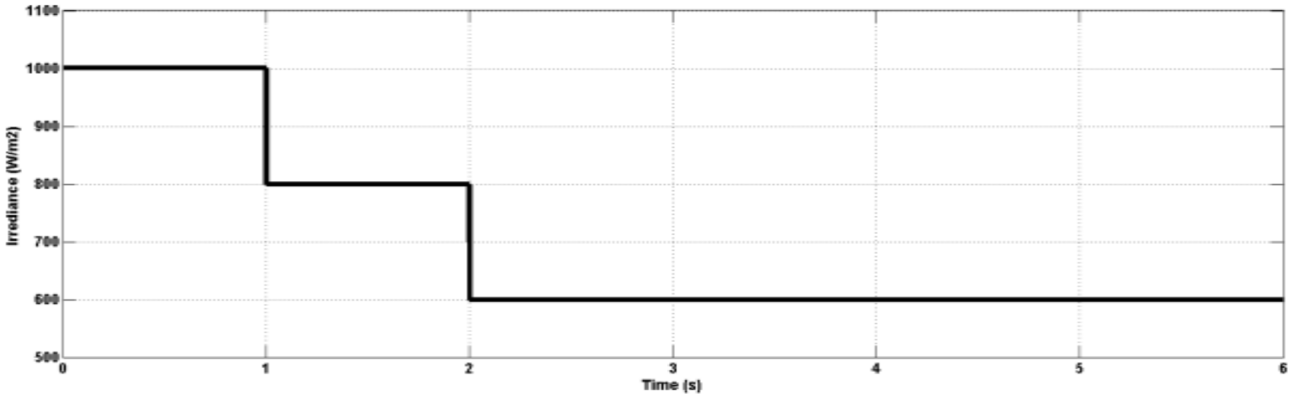

Figure 10. Irradiance variation.

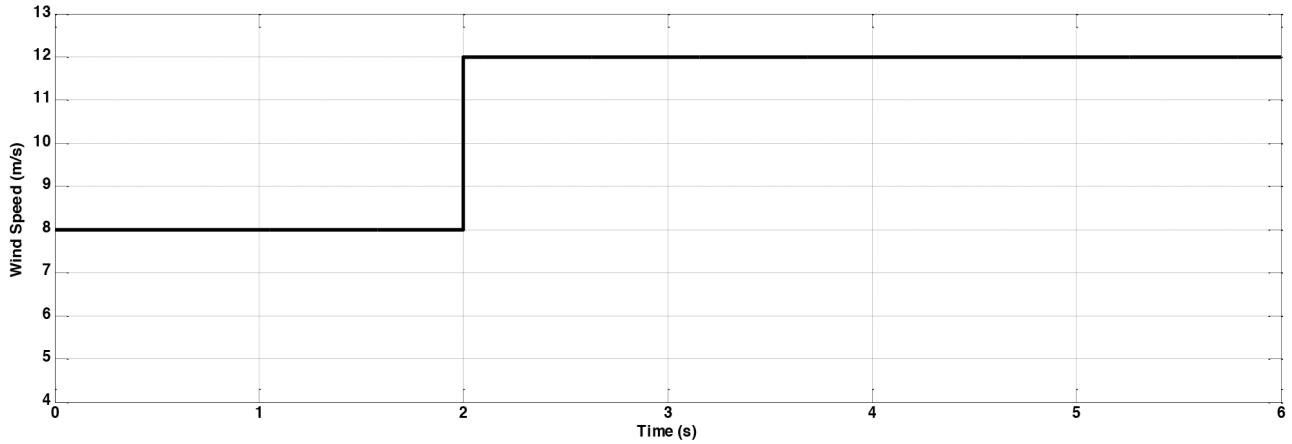

Figure 11. Wind speed variation.

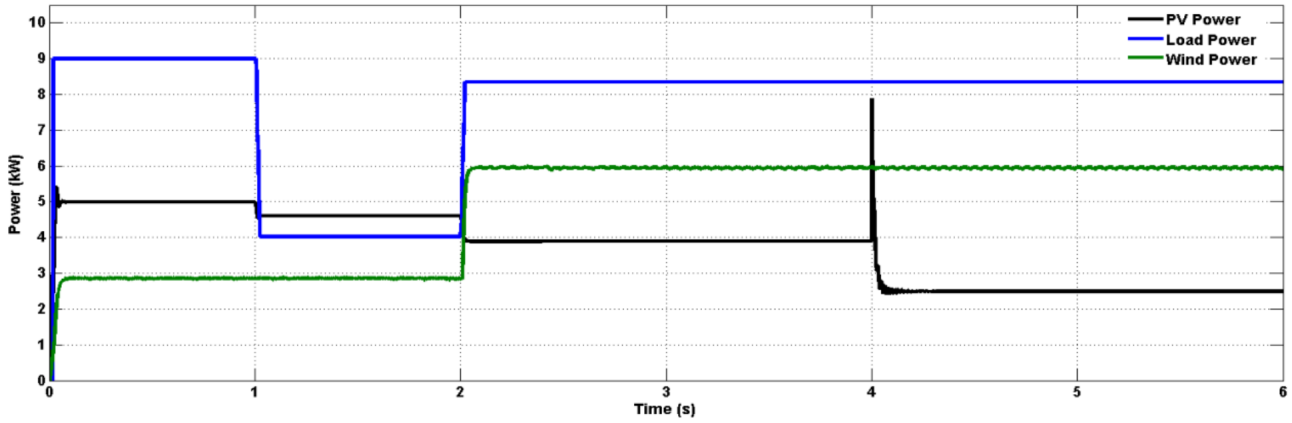

Figure 12. Variation of different powers.

After 1 s, load power demand is 4 kW, whereas wind and PV combined total power is 7.3 kW. Therefore, storage devices are in charging mode to compensate for the extra 3.3 kW of power from 1 s to 2 s as in Figure 12. Again from 2 s to 4 s the storage devices are in charging mode to compensate for the extra 1.6 kW of power when load demand is 8.3 kW and source power (wind and PV) is 9.9 kW. At 4 s, the SC is already fully

charged and the battery is on the point of overcharging. After 4 s, the battery goes into floating (disconnected) mode and the SC is in overcharging mode but is not able to compensate extra power. Therefore, OPPT control ensures maximum power output from the PV system up to 4 s when storage devices are able to compensate for the imbalanced power either in charging or discharging mode. However, from 4 s to 6 s, the PV system operates in the underrated condition and provides reduced output power from 3.9 kW to 2.3 kW, as required by the load demand, using the OPPT control technique.

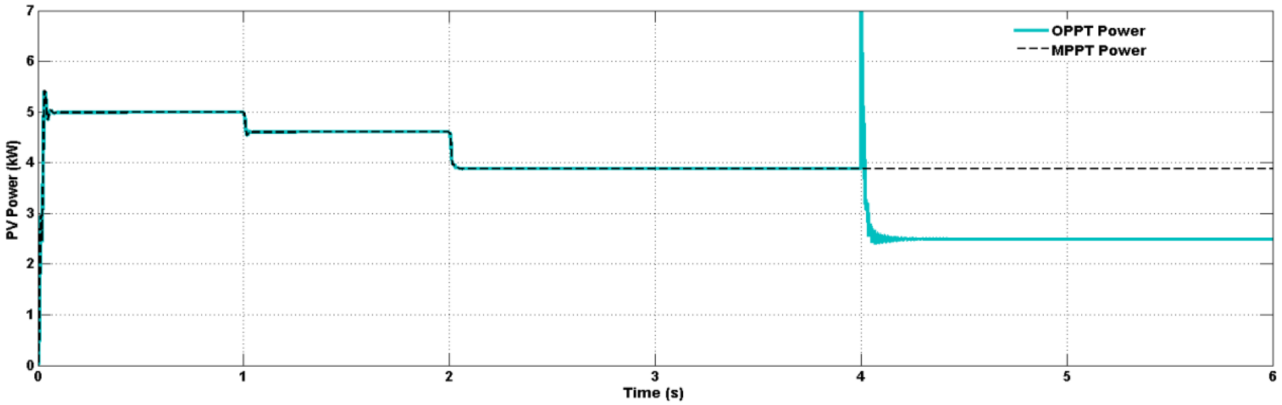

Figure 13. PV power output using OPPT and MPPT.

Figure 13 shows the PV output power using both OPPT and MPPT techniques in which it is evident that OPPT control works as MPPT control and provides maximum power when storage devices are able to regulate the power imbalance between the input source and output load from 0 s to 4s. Under the overcharging condition, storage devices are not able to regulate the power imbalance and hence OPPT control provides optimal power to meet the load demand instead of maximum power from 4 s to 6 s.

Figure 14 shows the power variation of storage devices as per charging/discharging mode to regulate the DC link voltage. Initially, storage devices are in discharging mode due to higher load demand as compared to the source power from 0 s to 1s. In charging mode, from 1 s to 4 s, when the source power is more than the load demand, the power of storage devices varies to compensate for the difference between the source and load powers for regulating the DC link voltage. From 4 s to 6 s, the battery is in floating (disconnected) mode and the SC is in overcharging mode.

Figure 15 shows the dynamics of the SC. The SC, due to its fast dynamics, compensates for power to regulate the DC link voltage, wherein it is clearly seen that the SC current is initially high and then reduces from 0 s to 1 s while the battery current increases.

Similarly, Figure 16 shows the dynamics of the battery from 1 s to 4 s. The SC has high charging current initially and then reduces while the battery charging current builds up slowly due to the slow dynamics of the battery.

From 4 s to 6 s, the battery is disconnected due to the overcharging condition but the SC remains connected in overcharging mode although it is not able to compensate power due to negligible overcharging current.

The DC link voltage regulates on 450 V using storage device control from 0 s to 4 s. OPPT control maintained constant DC link voltage from 4 s to 6 s when storage devices were disconnected, but MPPT control is not able to maintain constant DC link voltage as shown in Figure 17. Deviations in the DC link voltage around the regulation point demonstrate the fast dynamics of storage device control and illustrate the reasonably good

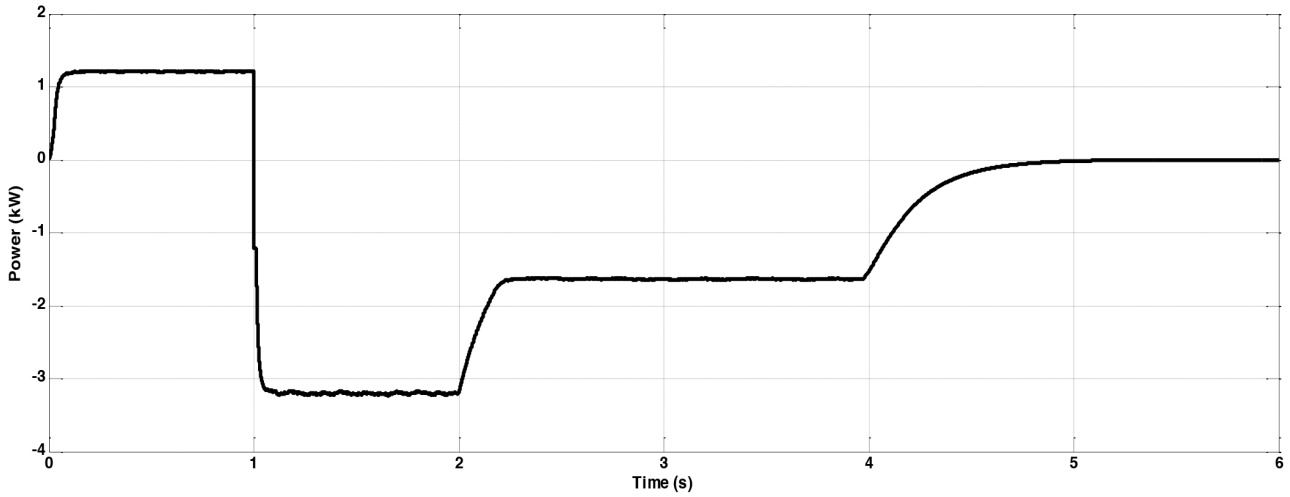

Figure 14. Variation of combined power of storage devices.

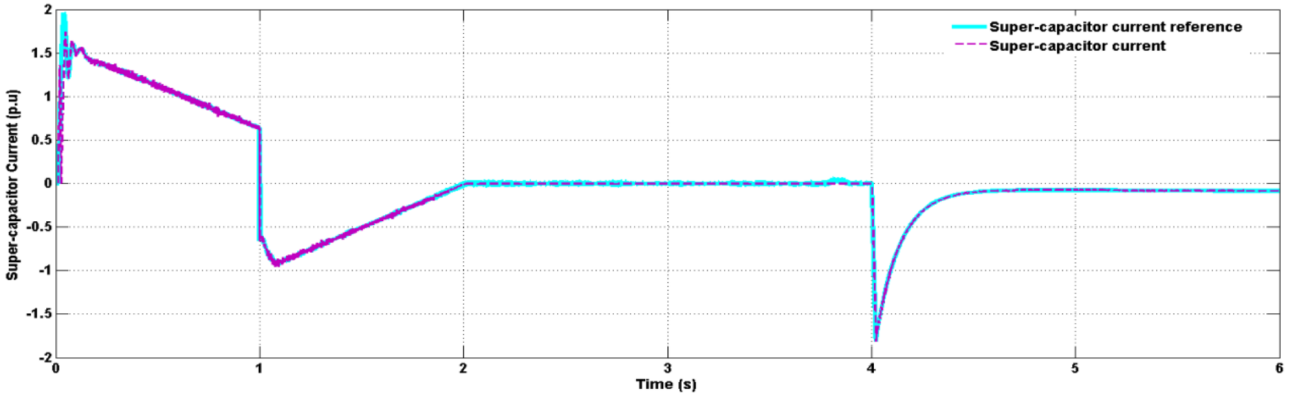

Figure 15. Supercapacitor current and reference current.

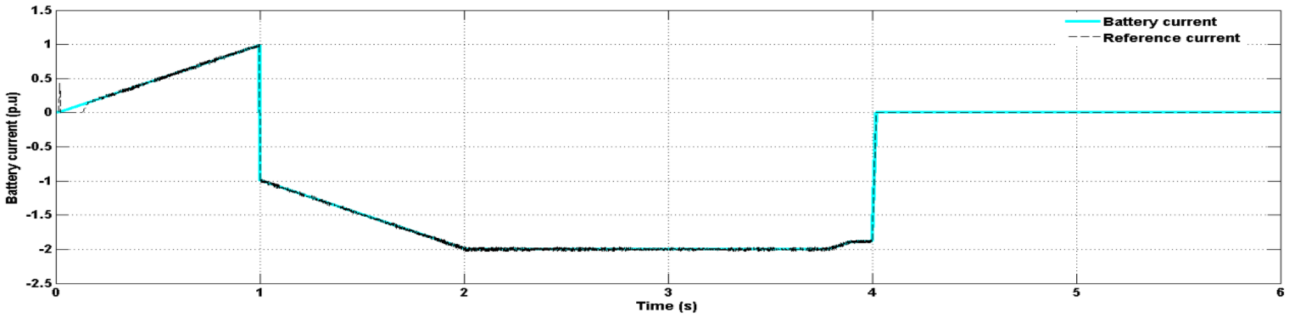

Figure 16. Battery current and reference current.

performance of OPPT control. Voltage variation is more from 4 s to 6 s as compared to the period from 0 s to 4 s due to the oscillation of power near the optimal point in OPPT control because of the inherent nature of the perturbation and observation technique.

As is evident from Figure 18, AC bus voltage is constant irrespective of changes in system conditions. At 1 s, even though the load and source inputs are changed, the AC bus voltage remains constant, which signifies

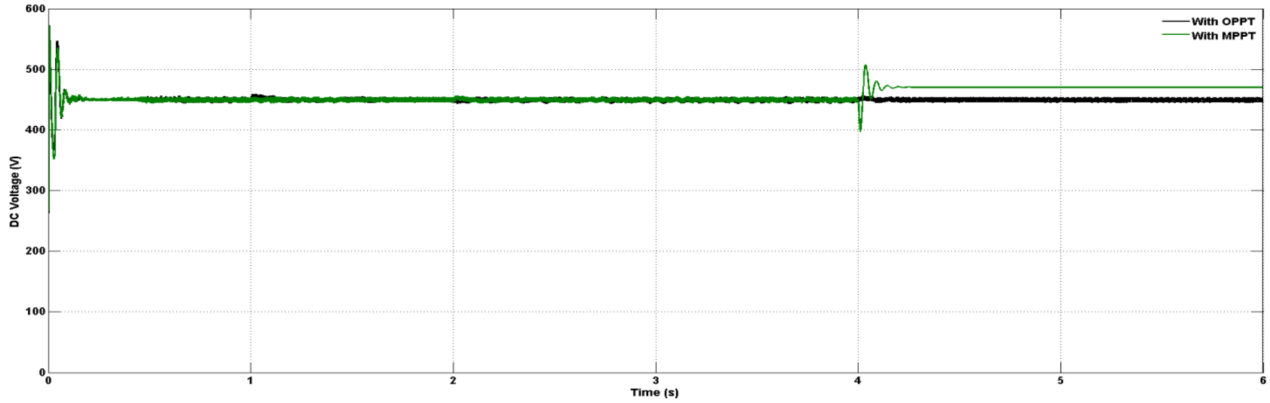

Figure 17. DC link voltage regulation.

the fast and improved dynamics of inverter control to be able to respond to small disturbances quickly.

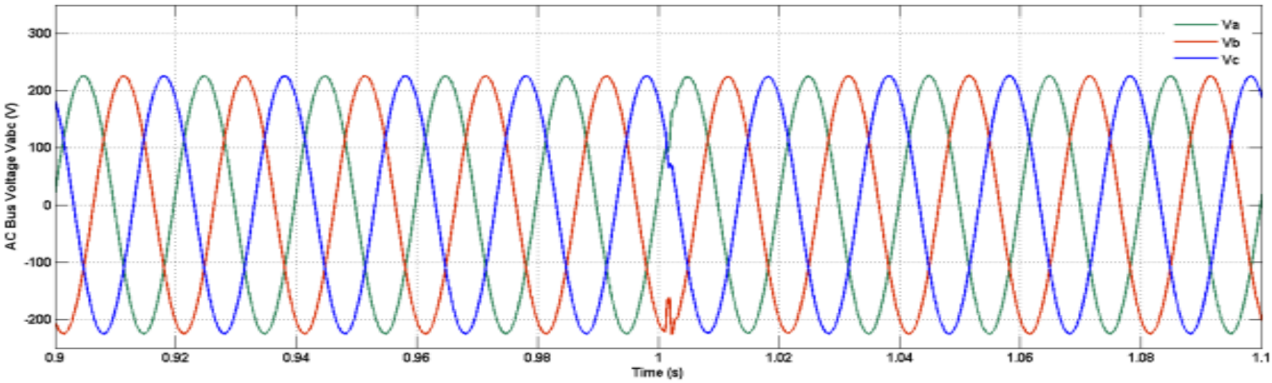

Figure 18. AC bus voltage.

Similarly, the three-phase AC bus current changes with change in load to meet the load demand as in Figure 19. At 1 s, there is change in the AC bus current corresponding to the change in load current to prevent the overvoltage condition, thereby resulting in improvement in transient condition at 1 s and establishing the improved performance of inverter control.

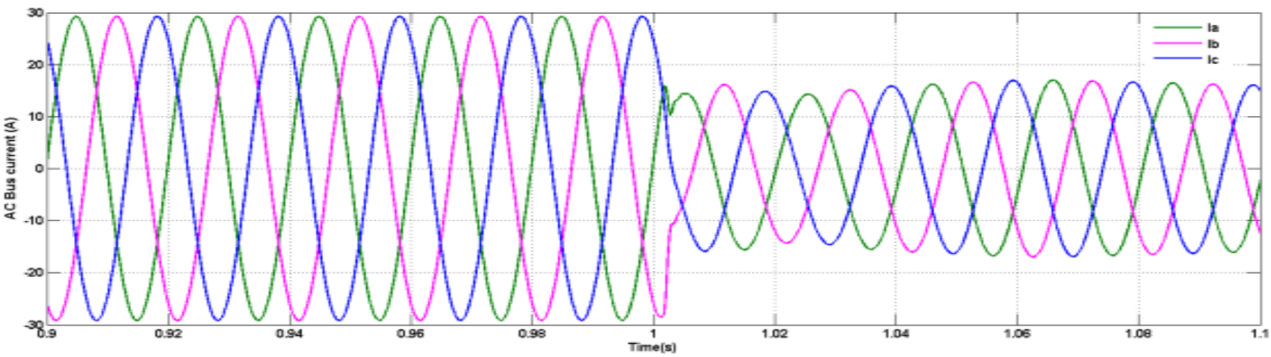

Figure 19. AC bus current.

5. Conclusion

This paper has proposed control strategies that include OPPT control and a novel control scheme for storage devices to improve the performance of the HRES under standalone conditions. Inverter control is also proposed to improve the overall performance of the system. OPPT control, as a replacement for MPPT, is proposed not just to track the maximum power but also to regulate the DC link voltage under overcharging conditions. PV system output is controlled by OPPT and the wind system is operated with MPPT control. The proposed OPPT control not only involves reduced cost; it also reduces the system complexity by eliminating the need for a controlled dummy load, thereby requiring less coordination of different controls involved. Novel control is proposed for storage devices, which reduces the tracking time and improves the dynamics to regulate the DC link voltage. Inverter control is proposed, which results in improved performance of the system at the AC bus. A complete hybrid renewable energy-based standalone system is simulated to study the effectiveness of the proposed control strategies. Results are presented and discussed to justify the improved performance with reduced components (dummy load removed) of the proposed novel control strategies.

References

[1] Sharma R, Suhag S. Survey on hybrid (wind/solar) renewable energy system and associated control issues. In: IEEE 2014 India International Conference on Power Electronics; 8–10 December 2014; Kurukshetra, India. New York, NY, USA: IEEE. pp. 1-6.

[2] Haruni AMO, Negnevitsky M, Haque ME, Gargoom A. A novel operation and control strategy for a standalone hybrid renewable power system. IEEE T Sustain Energy 2013; 4: 402-413.

[3] Nehrir H, Caisheng W, Strunz K, Aki H, Ramakumar R, Bing J, Zhixhin M, Salameh Z. A review of hybrid renewable/alternative energy systems for electric power generation: configurations, control and applications. IEEE T Sustain Energy 2012; 1: 22-26.

[4] Choudhury S, Mohapatra L, Rout PK. A comprehensive review on modeling, control, protection and future prospects of Microgrid. In: IEEE 2015 International Conference on Electrical, Electronics, Signals, Communication and Optimization; 24–25 January 2015; Visakhapatnam, India. New York, NY, USA: IEEE. pp. 1-6.

[5] Li YW, He J. Distribution system harmonic compensation methods: an overview of DG-interfacing inverters. IEEE T Ind Electron 2014; 8: 18-31.

[6] Guoyi XU, Lie XU, Liangzhong YAO. Wind turbines output power smoothing using embedded energy storage systems. J Mod Power Syst Clean Energy 2013; 1: 49-57.

[7] Ding G, Gao F, Zhang S, Loh PC, Blaabjerg F. Control of hybrid AC/DC microgrid under islanding operational conditions. J Mod Power Syst Clean Energy 2014; 2: 223-232.

[8] Malla SG, Bhende CN. Voltage control of stand-alone wind and solar energy system. Int J Elec Power 2014; 56: 361-373.

[9] Debnath D, Chatterjee K. Two-stage solar photovoltaic-based stand-alone scheme having battery as energy storage element for rural deployment. IEEE T Ind Electron 2015; 62: 4148-4157.

[10] Satpathy AS, Kishore NK, Kastha D, Sahoo NC. Control scheme for a stand-alone wind energy conversion system. IEEE T Energy Conver 2014; 29: 418-425.

[11] Kollimalla SK, Mishra MK, Narasamma NL. Design and analysis of novel control strategy for battery and super-capacitor storage system. IEEE T Sustain Energy 2014; 5: 1137-1144.

[12] Eghtedarpour N, Farjah E. Distributed charge/discharge control of energy storages in a renewable-energy-based DC micro-grid. IET Renew Power Gen 2014; 8: 45-57.

[13] Issa WR, Abusara MA, Sharkh SM. Control of transient power during unintentional islanding of microgrids. IEEE T Power Electr 2015; 30: 4573-4584.

[14] Patrick T, Moseley. Energy storage in remote area power supply (RAPS) systems. J Power Sources 2006; 155: 83-87.

[15] Gee AM, Dunn RW. Novel battery/supercapacitor hybrid energy storage control strategy for battery life extension in isolated wind energy conversion systems. In: IEEE 2010 International University Power Engineering Conference; 31 August–3 September 2010; Cardiff, UK. New York, NY, USA: IEEE. pp. 1-6.

[16] Yin M, Li G, Zhou M, Zhao C. Modeling of the Wind turbine with a permanent magnet synchronous generator for integration. In: IEEE 2007 Power Engineering Society General Meeting; 24–28 June 2007; Tampa, FL, USA. New York, NY, USA: IEEE. pp. 1-6.

[17] Villalva MG, Gazoli JR, Filho ER. Comprehensive approach to modeling and simulation of photovoltaic arrays. IEEE T Power Electr 2009; 24: 1198-1208.

[18] Figueres E, Garcera G, Sandia J, Gonzalez-Espin F, Calvo Rubio J. Sensitivity study of the dynamics of three phase photovoltaic inverters with an LCL grid filter. IEEE T Ind Electron 2009; 56: 706-717.

[19] Sathish Kumar R, Sathish Kumar K, Mishra MK. Dynamic energy management of micro grids using battery super capacitor combined storage. In: IEEE 2012 Annual Conference; 7–9 December 2012; India. New York, NY, USA: IEEE. pp. 1078-1083.

[20] Hedrick JK, Girard A. Control of Nonlinear Dynamic Systems: Theory and Applications. Berkeley, CA, USA: University of California, 2010.